Influence of Mg loss on the phase stability in Mg_2X (X = Si, Sn) and its correlation with coherency strain

Mohammad Yasseri[a,b,c], Kunal Mitra[a], Aryan Sankhla[a], Johannes de Boor[a], Eckhard Müller[a,b,c]

[a] Institute of Materials Research, German Aerospace Center (DLR), D – 51170 Koeln, Germany

[b] Institute of Inorganic and Analytical Chemistry, Justus Liebig University, Giessen, D – 35392 Giessen, Germany

[c] Center for Materials Research/LaMa, Justus Liebig University, Giessen, D – 35392 Giessen, Germany

https://doi.org/10.1016/j.actamat.2021.116737

Abstract

Understanding of the thermochemical stability of $Mg_2(Si,Sn)$ thermoelectric materials is crucial for their applicability in thermoelectric modules. A miscibility gap was reported for the quasi-binary Mg_2Si–Mg_2Sn series and the exact compositions of its limits are disputed. In this work we study the phase evolution and stability of $Mg_2Si_xSn_{1-x}$ with x = 0.5. Samples were annealed at 600 °C, 525 °C, and 450 °C both with and without excess elemental Mg in quartz ampules in order to manipulate the Mg vapor pressure. This led to two qualitatively different evolution routes of phase constitution, namely, (I) progressive phase separation and material degradation related to intense Mg loss accompanied by formation of side phases such as elemental Si and (II) much slower phase separation without formation of elemental precipitates when the sample was kept under Mg vapor atmosphere. Accordingly, XRD and EDAX gave evidence that the phase evolution and demixing behavior in magnesium silicide stannide depend sensitively on the amount and rate of Mg loss. We also observe stabilization of solid solutions against demixing by coherency strain and can show that the phase separation which will occur in thermodynamic equilibrium related to the miscibility gap, can be inhibited if Mg loss is suppressed. Then $Mg_2Si_{0.5}Sn_{0.5}$ shows improved stability at typical application temperatures (450 – 600 °C) which are far below the previously reported upper limit of the coherent miscibility gap (720 °C). The improvement of the phase stability of thermoelectric $Mg_2(Si,Sn)$ by controlling the Mg vapor pressure is of essential importance for long-term utilization of the material in thermogenerators at elevated temperatures.

1-Introduction

Thermoelectric materials are utilized to convert heat directly into usable electric power in thermoelectric generators (TEG) [1]. $Mg_2Si_xSn_{1-x}$ solid solutions are promising thermoelectrics and have attracted a lot of attention in recent years. In general, a highly efficient thermoelectric material has a low thermal conductivity (κ), a high Seebeck coefficient (S), and a high electrical conductivity (σ) at a given absolute temperature (T), as the thermoelectric conversion efficiency is related to the dimensionless figure of merit $zT = S^2\sigma T\kappa^{-1}$ [2]. $Mg_2Si_xSn_{1-x}$ thermoelectric solid solutions reach a high figure of merit zT_{max} of ~1.1–1.4 for n-type $Mg_2Si_{0.4}Sn_{0.6}$ due to convergence of the two lowest lying conduction bands [3-8]. Progress in material performance has also been shown for the p-type [9]. A miscibility gap in the phase diagram of the $Mg_2(Si,Sn)$ quasi-binary material system is reported where under certain conditions a phase separation can be observed [10, 11]. It is evident that the equilibrium boundary compositions formed as a consequence of the phase separation in $Mg_2Si_xSn_{1-x}$ are temperature dependent, though the reported results on the compositional range of the miscibility gap are disputed and contradicting (e.g. $0.4 < x < 0.6$ [10] and $0.34 < x < 0.92$ [12] at room temperature). A miscibility gap might open up a possibility for in-situ nanostructuring, hence, for further reduction of the thermal conductivity. Reduction of thermal conductivity due to a high concentration of grain boundaries formed as a consequence of phase demixing or second phase nanoinclusions and related local lattice strain will result in a larger zT provided that the detrimental influence of such structures on the carrier mobility is minor. For example, formation of nanodots by coherent precipitation of nanoseeds from complex chalcogenide compositions was shown to lead to strong enhancement of zT for LAST-18 compared to its base compound PbTe and other members of this material family [13-16]. As an example, in [17], phase separation occurred during cooling as a result of spinodal decomposition and nucleation, forming nanoinclusions (~3–10 nm). Nevertheless, demixing in a miscibility gap can also deteriorate thermoelectric properties, for example if a metastable solid solution within the gap would show beneficial features of the

electronic band structure which get lost as consequence of demixing. In $Mg_2Si_xSn_{1-x}$, the conduction bands show a desirable convergence, however, only for a limited compositional range, $0.3 < x < 0.4$ [3-7] which is located, according to some references, within the miscibility gap. Therefore, determining the exact boundaries of the miscibility gap in the $Mg_2Si_xSn_{1-x}$ system and understanding the phase separation mechanism is important for a controlled material optimization.

When holding single phase $Mg_2Si_xSn_{1-x}$ inside the miscibility gap at elevated temperature, phase separation may occur [18]. The phase separation mechanism can be either of spinodal decomposition or nucleation and growth [19]. According to the classical theory of the spinodal decomposition, if x in $Mg_2Si_xSn_{1-x}$ is within the chemical spinodal region of the miscibility gap, the solid solution is unstable and should undergo phase separation through spinodal decomposition spontaneously [20]. In contrast, if x is outside of the chemical spinodal region but inside the chemical binodal curve, the solid solution is metastable, and phase separation proceeds by a nucleation and growth mechanism [20], which requires to overcome an energy threshold for overcritical nucleation. This energy threshold could be decreased if there are structural defects or phase impurities, which can act as nuclei for phase precipitation. The microstructural signature of chemical spinodal decomposition is the formation of very fine lamellar/fringed structures (with spacing on the order of several angstroms to several nanometers), whereas in the nucleation and growth mechanism, precipitates are nucleated and coarsened inside a matrix [20]. However, the chemical spinodal ignores the effects of strain induced by coherent interfaces between the domains/grains of demixing phases [20, 21]. The coherency strain energy can have a significant contribution to the free energy of mixing in a disordered solid solution [20, 22], thus it can stabilize a metastable solid solution against demixing. This effect is not represented in the equilibrium phase diagrams [20, 22] which we will call here also incoherent phase diagrams as they are valid for demixed systems with incoherent grain boundaries that do not imply any relevant strain energy. On the contrary,

coherent phase diagrams show shifted features compared to the according equilibrium phase diagrams due to the effect of strain energy related to a lattice mismatch at the coherent boundaries. Daok et. al. reported a coherent spinodal line which was different from the chemical spinodal line in the PbS-PbTe material system [20]. There, coherency strain was caused by a large lattice mismatch (8.5% [23, 24]) of the constituent compounds (PbS and PbTe) [22]. The maximum temperature of the experimental miscibility gap in PbS-PbTe (610 K) was lowered by 1160 K compared to the corresponding temperature of the incoherent miscibility gap (1770 K) [20].

In most of the previous reports the composition of $Mg_2Si_{0.5}Sn_{0.5}$ is supposed to be within the miscibility gap in the Mg_2Si–Mg_2Sn phase diagram at temperatures below the upper limit of the miscibility gap (at 700 – 800 °C) [10, 12, 25]. Therefore, single phase $Mg_2Si_{0.5}Sn_{0.5}$ is supposed to get formed only if the synthesis temperature is above the upper limit of the miscibility gap (under 1 atm). However, in contrast to all predicted phase diagrams, there are several reports on the formation of single phase $Mg_2Si_{0.5}Sn_{0.5}$ [26-28], which were prepared by hot-pressing (under e.g. 80 MPa) at temperatures lower than the upper limit of the chemical miscibility gap calculated in theoretical studies (at 700 – 800 °C) [10, 12]. In our previous work [29], experimentally, we proved complete solubility at 700 °C for $Mg_2Si_xSn_{1-x}$ compositions with $x \leq 0.6$, which were formed under 64 MPa in DSP (Direct Current Sintering Press). This includes the compositions with the best thermoelectric properties for both n- and p-type material ($Mg_2Si_{0.5}Sn_{0.5}$ – $Mg_2Si_{0.3}Sn_{0.7}$) [4, 30]. Also, Yi et al. [18] could obtain a single phase $Mg_2Si_{0.7}Sn_{0.3}$ solid solution at 720 °C through homogenization of Mg_2Si and Mg_2Sn particles while sintering by SPS (Spark Plasma or Current-assisted Pressure Sintering). They carried out thermodynamic analysis as well as phase-field microstructure simulations for the Mg_2Si-Mg_2Sn system and suggested that the strain energy due to coherency suppresses the spinodal decomposition and prevents phase separation at 720 °C [18, 31].

It is commonly reported in the literature that the $Mg_2(Si,Sn)$ material system suffers from Mg loss above 500 °C [32-34]. It is often reported in the literature that the phase separation in the miscibility gap is followed by the formation of elemental Si, elemental Sn or an Sn-Mg melt due to Mg loss from $Mg_2(Si,Sn)$ [10, 32, 34, 35]. The ternary phase diagram [36] helps to verify the validity of several decomposition mechanisms proposed in literature. Yin et al. [37] suggested that a peritectic reaction occurs at 550 °C with the formation of a Si-rich $Mg_2(Si,Sn)$ solid phase and a Sn-rich Sn-Mg liquid phase, however this is not consistent with [36]. According to Yin et al. [37], the Si-rich $Mg_2(Si,Sn)$ transforms into volatile Mg and elemental Si [36]. Also, the Sn-Mg liquid phase is not stable at high temperatures but decomposes into Mg and Sn with Mg evaporating quickly [37]. Nevertheless, according to [36], decomposition of Sn-Mg into Sn and Mg is not possible alone since there is $Mg_2(Si,Sn)$ existent over all relevant temperatures, thus Sn-Mg should decompose into an Sn-rich Sn-Mg liquid and $Mg_2(Si,Sn)$. These processes are detrimental for $Mg_2(Si,Sn)$ as they indicate low thermal stability for the material system related to the Mg loss.

The aim of the current study is to demonstrate practically that the atmosphere surrounding a $Mg_2(Si,Sn)$ sample has a strong impact on stability and evolution of the phase constitution. As a consequence, this opens an option to stabilize the material, e.g. to be used for long-term operation in thermoelectric modules, by control of the ambient Mg vapor pressure. Extending this conclusion might lead to advanced material processing where in a first step with controlled Mg depletion phase, demixing is initiated to a well-defined degree. It improves the thermoelectric performance by enhanced grain boundary scattering whereas then this status is stabilized and further degradation, in particular precipitation of metallic impurity phases, is blocked by operating the material at a stable Mg vapor atmosphere preventing further Mg loss.

In order to study the material behavior under two essentially different ambientes, two groups of $Mg_2Si_xSn_{1-x}$ samples with $x = 0.5$ were synthesized and annealed at 600 °C, 525 °C, and 450

°C. The effect of surrounding Mg vapor pressure on the phase constitution of the $Mg_2Si_xSn_{1-x}$ samples is studied using XRD and SEM/EDAX. We demonstrate that providing some Mg vapor around the samples together with using boron nitride (BN) coating can suppress material degradation and can block the phase separation according to the miscibility gap. We assume that coherency strain is a main factor that can preserve the material from phase separation over the miscibility gap down to temperatures far below the previously reported upper limit of the miscibility gap.

2- Experimental

$Mg_2(Si,Sn)$ samples were synthesized by mechanical alloying using a high-energy ball mill (SPEX 8000D Shaker Mill), followed by a compaction step in a direct-current sintering press (DSP 510 SE, Dr. Fritsch GmbH, Fellbach, Germany) [4, 30, 38, 39]. The samples with a nominal composition of $Mg_{2.1}Si_{0.4925}Sb_{0.075}Sn_{0.5}$ contained antimony as a dopant [31, 40] to achieve optimized thermoelectric performance [28]. Excess Mg was used to compensate Mg loss. For brevity, we refer to this composition as $Mg_2Si_{0.5}Sn_{0.5}$ in the following.

The role of the Sb dopant on the phase equilibria and kinetics of the phase separation of $Mg_2(Si,Sn)$ is not studied in this work. The authors acknowledge that any additional element such as Sb can play a role to change the Si and Sn solubility limits in $Mg_2Si_xSn_{1-x}$ if its amount is considerable. The additional element makes the material system quasi-ternary. The aim of the current study is to shed light upon the phase separation mechanism and its preconditions. A detailed study of the effect of the Sb content is beyond the scope of the current study. However, we kept the Sb content constant for the annealing experiments to keep the possible effect of Sb constant. As the Sb concentration in the samples is very low, also a related shift in the thermodynamic properties is expected to remain small.

The details of the synthesis procedure can be found in [4]. Sintering at a holding temperature of 700 ˚C for 60 min under a uniaxial pressure of 64 MPa yielded pellets of homogeneous

$Mg_2Si_{0.5}Sn_{0.5}$ phase with high purity [29, 38]. To track the material degradation and the phase segregation according to the miscibility gap, the samples were annealed at 600 °C, 525 °C, or 450 °C for different time durations and under different annealing conditions (see Table 1). The samples were sealed in quartz ampules under Argon with a pressure of 560 mbar. As a first protection measure against Mg loss, the samples were coated with a layer of boron nitride (BN) by brush painting before sealing (annealing condition I). Despite, some Mg was evaporating from the samples during heat treatment and reacted with SiO_2 of the ampule forming a thin layer of Mg_2Si on the ampule wall [41]. As a second annealing condition, to further reduce the rate of Mg evaporation, the BN-coated samples were sealed in quartz ampules together with 0.5 g of Mg flakes which provided some Mg vapor pressure in the annealing environment (annealing condition II).

Table 1. Sample number, annealing time and preparation procedure.

Sample Code	**Annealing Temperature (˚C)**	**Annealing Time (days)**	**Annealing Environment**	**Status of the Sample after Annealing**
I-600-07	600	7	Ar	Strong Mg loss, elemental Si, Sn observed
II-600-05	600	5	Ar + Mg	No elemental Si, Sn observed
II-525-05	525	5	Ar + Mg	No elemental Si, Sn observed
I-450-30	450	30	Ar	No elemental Si, Sn observed

The duration of the heat-up ramp to the annealing temperature for all of the samples was 24 hours, to avoid thermal shock of the samples while heating. After annealing the samples for the time durations mentioned in Table 1, the ampules were taken out from the furnace and cooled down in room temperature air.

X-ray diffraction patterns were taken on powders and sample pellets utilizing a Siemens D5000 Bragg−Brentano diffractometer with a secondary monochromator, and a Bruker D8-advanced

diffractometer with Cu-K_α radiation (1.5406 Å) in the 2θ range of 20° − 80° with a step size of 0.01°.

Backscattered electron images were taken using a Zeiss Ultra 55 SEM with a Zeiss QBSE detector, also equipped with an Oxford energy dispersive X-ray (EDAX) detector (PentaFETx3). Acceleration voltages of 8, 15, and 25 kV were selected for the EDAX measurements. Using a formula given in [42] for estimation of the EDAX spatial resolution in each phase of the multiphase materials, different values of the spatial resolution are obtained for Mg, Sn, Si, Mg_2Sn, and Mg_2Si, and $Mg_2Si_{0.5}Sn_{0.5}$. The estimated spatial resolutions of different phases are mentioned in Table 2.

Table 2. Estimated spatial resolution for different phases and acceleration voltages.

	Phase	**Acceleration Voltage**		
		8 kV	**15 kV**	**25 kV**
Spatial Resolution (µm)	**Mg**	1.16	3.43	8.16
	Si	0.83	2.53	6.06
	Sn	0.23	0.76	1.89
	Mg_2Si	0.98	2.96	7.09
	Mg_2Sn	0.45	1.57	3.90
	$Mg_2Si_{0.5}Sn_{0.5}$	0.55	1.91	4.75

3- Results

Details on the phase evolution of $Mg_2Si_xSn_{1-x}$ during high energy ball milling are discussed in [4]. Fig. 1 shows the XRD patterns of a sintered sample (as-pressed) as well as of samples annealed at 600 °C for 7 and 5 days, respectively, under different annealing atmospheres. The square root of intensities is plotted versus 2θ to enhance the visibility of the impurity phases. As discussed in our previous study [29], the X-ray diffraction pattern of the sample sintered for

1 h at 700 ˚C indicates a highly pure structure (disregarding a minor MgO peak at 2θ = 42° and the formation of a homogenous $Mg_2Si_{0.5}Sn_{0.5}$ phase. For the sample annealed at 600 ˚C for 7 days (sample I-600-07), there are two main groups of XRD peaks corresponding to Si-rich and Sn-rich Mg_2(Si,Sn) compositions. The right-shifted peaks, corresponding to a higher Si to Sn ratio compared to the initial $Mg_2Si_{0.5}Sn_{0.5}$ matrix have the sharpest shape. Furthermore, there are some peaks for sample I-600-07 corresponding to elemental Sn and Si whereas no elemental Si and Sn was recognized in the XRD pattern of the sample as-pressed at 700 °C for 1 h. This strongly suggests that some elemental Si and Sn precipitated in the sample as a result of annealing at 600 °C under condition I. We believe that the precipitation of elemental Si and Sn in the sample is due to the continuous Mg loss from the sample. The elements appear as a result of the limited solubility of overstoichiometric *X* (Si, Sn) in Mg_2X. The XRD pattern of the sample II-600-05 shows mainly peaks corresponding to Si-rich Mg_2X compositions close to the starting composition together with small peaks corresponding to Sn-rich Mg_2X secondary phases (we will call Si-rich Mg_2X the matrix phase in the following because we see that this is the largest volume fraction from which other phases in small fractions precipitate). The mean position of the matrix peaks in this sample is closer to the peak positions of the starting composition and farther from the corresponding peaks of the standard Mg_2Si pattern compared to I-600-07 for which no extra Mg flakes were annealed together with the sample. The XRD pattern of the sample II-600-05 (annealed together with Mg flakes) does not show any formation of elemental Si or Sn. Providing Mg flakes into the ampule leads to an increased Mg vapor pressure near the sample. This presumably reduced Mg loss from the sample and prevented precipitation of Si-rich and Sn-rich decomposition products. Also, the reduced Mg loss leads to a smaller shift of the Mg_2X matrix composition.

The XRD patterns of the sample II-525-05 and the sample I-450-30 indicate a highly pure structure (disregarding the minor MgO peak at 2θ = 42°) and a homogenous $Mg_2Si_{0.5}Sn_{0.5}$ phase. The patterns show no formation of elemental Si or Sn. Furthermore, there is no obvious

peak splitting indicating any phase separation in these samples which could possibly occur due to the miscibility gap in the Mg_2X series.

The inset on the right side of Fig. 1 shows an enlarged view of the (220) peak (37° – 41°) of the samples annealed at 600 °C. After annealing, there is a superposition of several peaks in form of two broad but distinct peaks corresponding to Sn-rich compositions coexisting in the sample I-600-07 after annealing. The coexistence of different Sn-rich compositions might be due to the coexistence of different conditions (different degree of Mg loss) at different, distant places in the sample.

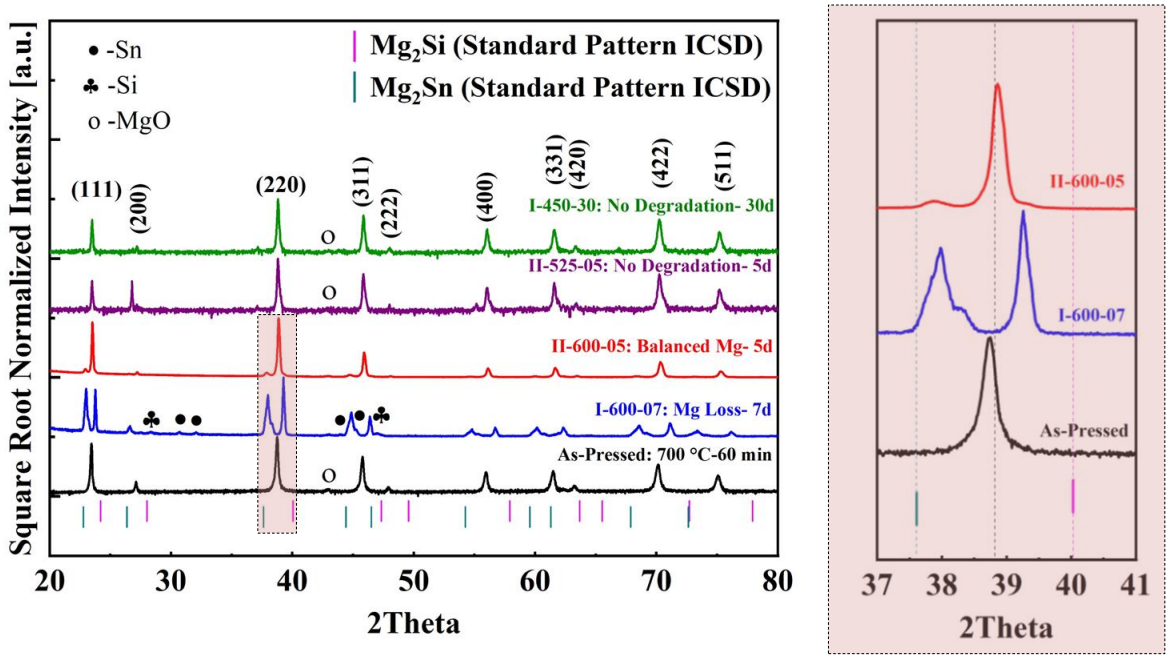

Figure 1. XRD patterns of the pressed $Mg_2Si_{0.5}Sn_{0.5}$ sample as well as the samples annealed at 600 °C, 525 °C, and 450 °C under the conditions given in Table 1. A phase separation is obvious for the annealed samples. Pink and blue bars at the bottom show standard patterns of Mg_2Si and Mg_2Sn, respectively. The magnification (right) shows an enlarged view of the (220) peak of the samples annealed at 600 °C. The black dashed line in the inset indicates the position of the respective peak for $Mg_2Si_{0.5}Sn_{0.5}$ according to Vegard's law.

Table 3 shows the mean values of the Si-rich and Sn-rich compositions determined from the XRD results (Figure 1). The mean compositions were estimated from the lattice constants of the Si-rich Mg_2X matrix, and Sn-rich Mg_2X phases (where existing) based on Vegard's law.

The lattice constants of Mg_2Si and Mg_2Sn were taken from the literature reports ([43] and [44], respectively). The calculated mean value of the composition of the as-pressed sample (x = 0.49 for Sb-doped $Mg_2Si_xSn_{1-x}$) is in close agreement with the nominal composition ($Mg_2Si_{0.4925}Sn_{0.5}Sb_{0.0075}$). We also note that obtained lattice constant of the as-pressed sample (a = 6.559 Å) is in good accordance with the literature value for the lattice constant of an undoped $Mg_{2-\delta}Si_{0.5}Sn_{0.5}$ sample (a = 6.559 Å) reported recently by Kato et al. [45], supporting the credibility of the chosen approach.

Table 3. Estimated mean values of $Mg_2Si_xSn_{1-x}$ lattice constants and respective compositions before and after annealing; obtained from XRD peak positions at $2\theta = 37° – 40°$ (Figure 1).

Sample	**Lattice Constant(s) (Å)**	**Composition(s) (x)**	**Status**
As-Pressed	6.559	0.49	Matrix
I-600-07	6.714	0.12	Sn-rich
	6.648	0.28	Sn-rich
	6.497	0.63	Matrix
II-600-05	6.550	0.12	Sn-rich
	6.713	0.51	Matrix
	6.473	0.69	Si-rich
II-525-05	6.559	0.49	Non-demixed
I-450-30	6.558	0.49	Non-demixed

It should be mentioned that the values in Table 3 are calculated disregarding the effect of the Sb dopant. We assume that the concentration of Sb in $Mg_2Si_{0.5}Sn_{0.5}$ is below its solubility limit based on our previous study [8] where up to 1.5 mole% Sb was added but no Sb-rich secondary phases like, e.g., Mg_3Sb_2 were observed. Therefore, in principle, a shift of the lattice constant due to the Sb addition must be expected. However, we suppose that for 0.75 mole% Sb doping, the changes of the lattice constants are negligible in agreement with previous results in the literature (compare e.g. [46, 47] with [48]). Also, the lattice constant reported in Table 3 for the as-pressed $Mg_2Si_{0.5}Sn_{0.5}$ sample doped with 0.75 molar percent Sb (a = 6.559 Å) is very close to the lattice constant of the undoped $Mg_{2-\delta}Si_{0.5}Sn_{0.5}$ obtained by Kato et al. (a = 6.556 Å) [45]. Figure 2a and b show SEM images of an as-pressed sample sintered at 700 °C for 1 h under 64 MPa. The microstructure proves a quite uniform homogenous phase. Figure 2c-e show

backscattered electron (BSE) SEM images as well as EDAX results of the sample I-600-07. The SEM images show that there are mainly four distinct regions in the sample which have different gray values, labeled as black (B), dark gray (D), light gray (L), and white (W). The morphology of the regions of the annealed sample differs completely from that of the as-pressed sample before annealing where a homogeneous $Mg_2Si_{0.5}Sn_{0.5}$ phase was observed. Several EDAX point spectra were obtained from B, D, L, and W regions distributed over the whole sample. Repeatedly, EDAX point analysis revealed relatively close values of atomic percentage of the constituents (Mg, Si, Sn) in each of the regions, respectively, all over the sample. The EDAX results obtained from the distinct sample regions are shown in the graphs below the SEM images. The regions can be identified as elemental Si (black), Si-rich Mg_2X with a mean composition of $Mg_2Si_{0.6}Sn_{0.4}$ (dark gray), Sn-rich Mg_2X with a mean composition of $Mg_2Si_{0.1}Sn_{0.9}$ (light gray), and elemental Sn (white). Elemental Si and Sn are formed due to Mg loss. Probably, while annealing, after Sn-rich Mg_2X has started to precipitate, it decomposes further into Si and an Sn-Mg melt. The W regions are remnant of that Sn-Mg melt, either in form of metastable Sn which dissolved some Mg, or as a fine-scaled eutectic of Mg_2Sn and elemental Sn, or as elemental Sn. Both the latter options are in accordance with the evidence of elemental Sn in the XRD result of the I-600-07 sample (see Fig. 1). Also, in Fig. 2e, in the EDAX of Si precipitates (B), there are scattering data indicating some amount of Mg and Sn inside or locally adjacent to this phase. Similarly, the spectrum indicated that the Sn-rich (W) regions contain some Si and Mg. The apparent discrepancy between the EDAX point analysis and XRD results of the thermodynamically expected pure elemental Sn and Si [36] are presumably due to the limited spatial resolution of EDAX. For example, the spatial resolution in the Si (B) region is 2.5 µm with the acceleration voltage used (15 kV). In the EDAX point analysis, some interfering information from neighboring grains with coexisting phases will be reflected in the results, if the grain size of the phase of interest is within or smaller than the EDAX spatial resolution of that individual phase. The size of Si particles measured in Fig. 2c

(spectra number 1 and 5) is close to the estimated spatial resolution (2.5 μm); therefore, some information from phase domains neighboring the B region might influence the EDAX results. The coexistence of Si-rich ($Mg_2Si_{0.6}Sn_{0.4}$) and Sn-rich ($Mg_2Si_{0.1}Sn_{0.9}$) Mg_2X compositions in immediate mutual local neighborhood indicates phase separation in the Mg_2X isopleth at 600 °C similar to what was shown by XRD (see Figure 1). The two co-existing $Mg_2Si_xSn_{1-x}$ phases might obviously form due to existence of a miscibility gap at 600 ˚C when the material undergoes Mg loss.

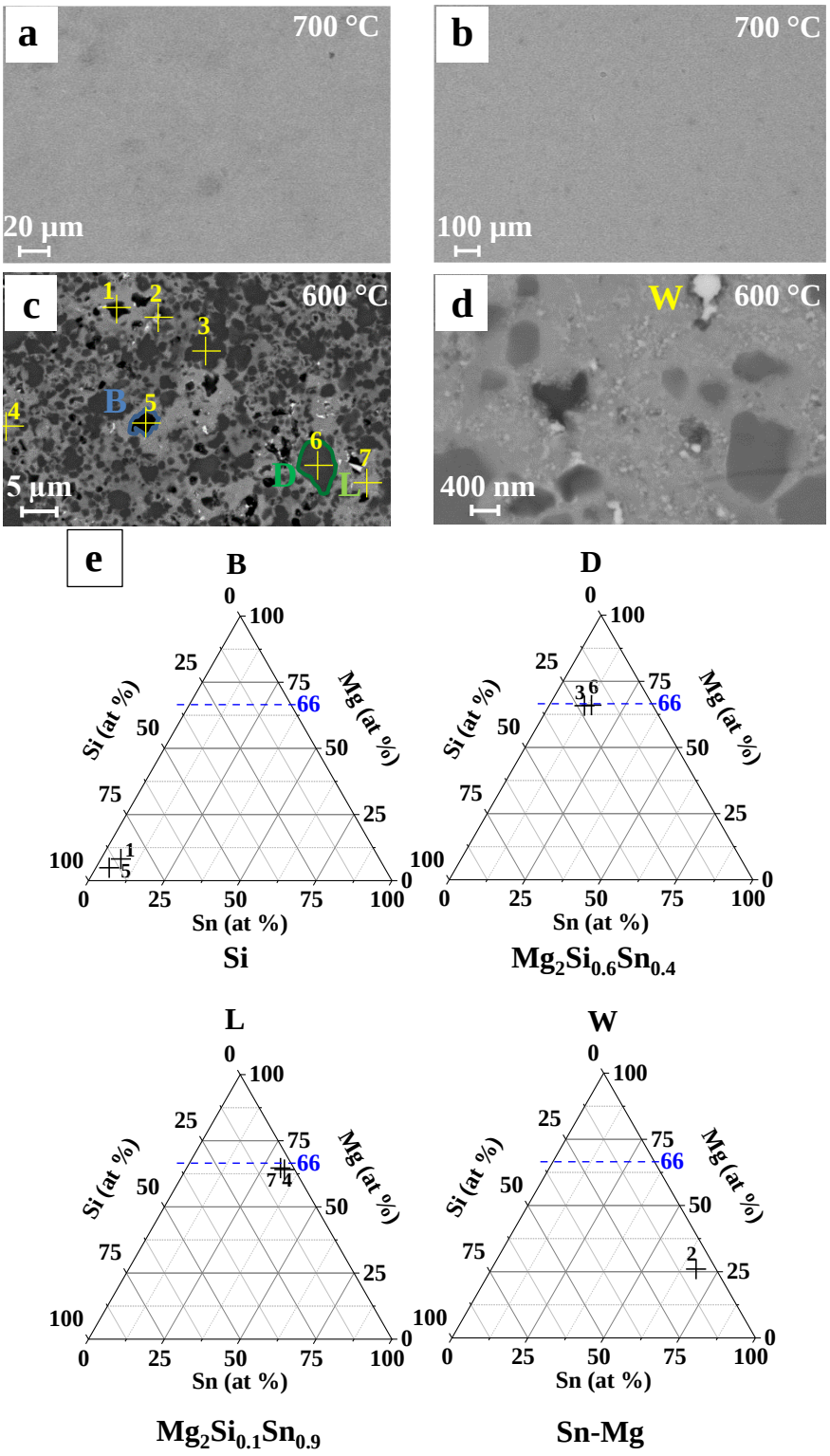

Figure 2. (a) and (b) SEM images of a $Mg_2Si_{0.5}Sn_{0.5}$ sample sintered at 700 °C for 60 min under 64 MPa taken with different magnifications. BSE-SEM (c and d) and EDAX results (e) of the sample annealed at 600 ˚C under Mg-deficient atmosphere for 7 days (I-600-07). The material contains four main phases after annealing, namely: elemental Si (Black, e.g. No. 1 and 5), Si-rich with a mean composition of $Mg_2Si_{0.6}Sn_{0.4}$ (Dark gray, e.g. No. 3 and 6), Sn-rich with a mean composition of $Mg_2Si_{0.1}Sn_{0.9}$ (Light gray, e.g. No. 7), and Sn-rich Sn-Mg melt / elemental Sn (White). Measured points and the corresponding EDAX results are indicated by numbers in the SEM figure and the ternary diagrams.

Figure 3 shows the SEM image of the sample II-600-05 and corresponding EDAX results (point spectra). There are some white regions at the grain boundaries of the matrix grains. EDAX results show constant compositions within the grains but some scattering in the Si/Sn ratio at the whitish regions though the size (thickness) of these regions is beyond the limit of the EDAX spatial resolution. Considering the XRD results of the same sample II-600-05 (See Figure 1), where a small peak of a Sn-rich Mg_2X composition distinct from the matrix peak was revealed, we conclude that the precipitated whitish regions are Sn-rich compositions whereas the matrix remained close to the starting composition. The matrix preserves its grain morphology but according to the XRD pattern it shifted from $Mg_2Si_{0.5}Sn_{0.5}$ to a composition with a slightly higher Si to Sn ratio. There is no elemental Si or Sn formed in this sample.

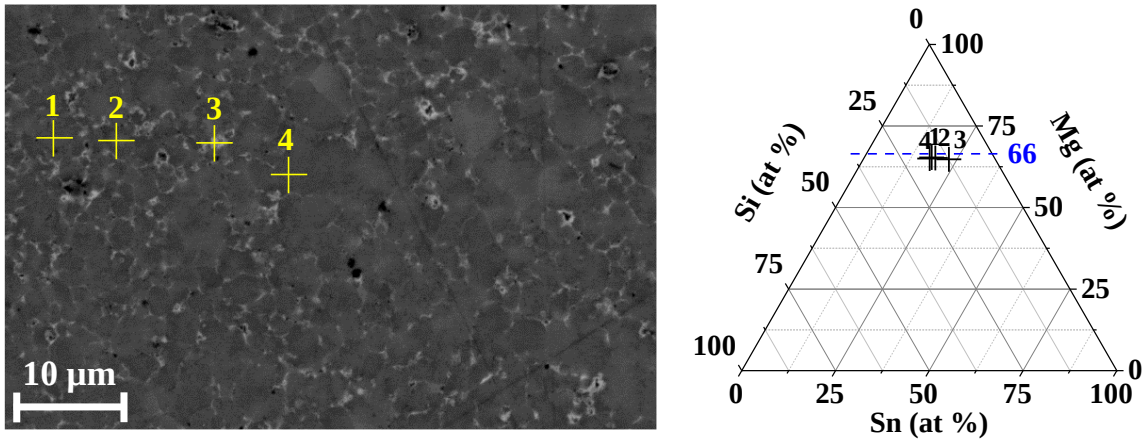

Figure 3. BSE-SEM and EDAX results of the sample annealed at 600 ˚C for 5 days with Mg flakes (II-600-05). EDAX point analysis indicates a slight scattering in Si and Sn atomic percentages due to the beginning phase separation. Measured points and the corresponding EDAX results are indicated by numbers in the SEM figure and the ternary diagram.

Figure 4 shows SEM images and corresponding EDAX results of the samples II-525-05 and I-450-30. The sample annealed at 525 °C (II-525-05; with BN coating and Mg flakes; Figure 4a and 4b) shows a quite homogenous morphology with a small variation in atomic percentage of Si and Sn in different regions of the sample indicating that the sample has not demixed. According to the EDAX results there is no clear indication of Mg loss in this sample (no formation of elemental Sn or Si). The results indicate that the Mg vapor pressure around the

samples while annealing which was maintained by additional Mg flakes in the ampule as well as by the barrier formed by BN coating suppressed the Mg loss from the sample. Preventing Mg loss slowed down the miscibility gap induced phase segregation. The SEM image of the sample annealed at 450 °C for 30 days (I-450-30) without Mg flakes but with an adequate BN coating shows a homogenous sample without formation of elemental Si or Sn or any phase separation. The results are in agreement with [49], where Bi-doped $Mg_2Si_{0.3}Sn_{0.7}$ samples showed a high thermal stability at 450 °C using BN coating.

In contrast to the results presented for the samples annealed at 600 °C with high Mg loss, in the case of samples annealed at 525 °C and 450 °C, we observe relatively homogeneous grey scale images containing only a few light and dark dots, and the EDAX results show low scattering of the Si/Sn ratio. This is in accordance with the XRD results (see Figure 1) indicating no phase separation in the course of these experiments.

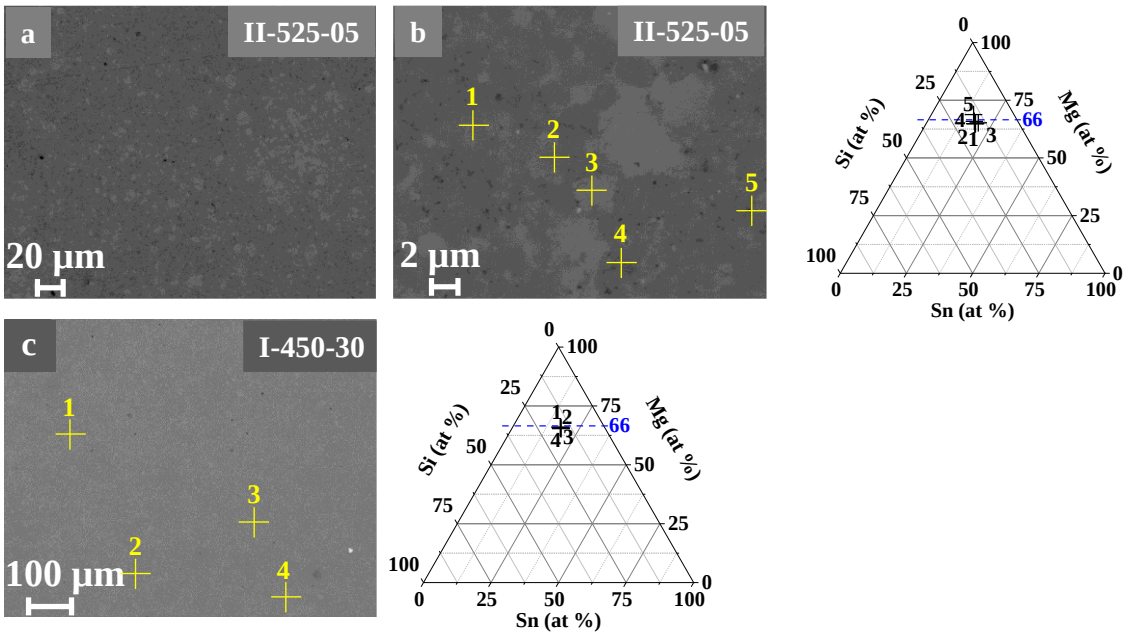

Figure 4. (a) BSE-SEM of the sample annealed at 525 ˚C (with Mg flakes and BN coating) for 5 days (II-525-05), (b) BSE-SEM (higher magnification) and EDAX results of the same sample, (c) BSE-SEM and EDAX for the sample I-450-30, annealed at 450 ˚C (without Mg flakes but with an adequate BN coating) for 30 days. Measured EDAX points are indicated by numbers in the SEM figure and the ternary diagrams.

4- Discussion

$Mg_2Si_{0.5}Sn_{0.5}$ samples have been homogenized at 700 °C while sintering under pressure, where a solid solution was formed before they were annealed at lower temperatures [29]. In the light of the conclusions by Yi et al. [18] we believe that the $Mg_2Si_{0.5}Sn_{0.5}$ solid solution is metastable at 700 °C due to the strain energy contributions to the free energy, suppressing the (otherwise) expected demixing due to the incoherent miscibility gap [29]. The crystal structure of the crystallites of the high energy ball-milled powder contains many lattice defects and a large amount of strain is present [50]. The defects are caused by the heavy mechanical impact of the milling process and represent mainly faults in the periodic order of the lattice rather than a global shift of stoichiometry. Thus, the ball-milled powder represents a highly excited state of the crystalline lattice in the already formed solid solutions. While pressing the pellet at 700 °C under axial pressure (64 MPa), these defects annihilate locally by re-establishing lattice periodicity. We suppose that reordering under (axial) pressure results in widely coherent grain boundaries. For example, it was previously reported that for Mo-Ni alloys solid solution formation occurs by sintering through diffusion-induced grain boundary migration. If a thin liquid film exists at the grain boundaries of the solute species, the grain boundaries migrate only by formation of a coherency strain in the diffusion zone ahead of the migrating boundaries [51-54]. Similarly, we believe that under such sintering conditions at 700 °C coherent interfaces could likewise form between the grains of $Mg_2(Si,Sn)$, also assisted by the applied pressure. The coherency strain related to the lattice mismatch between different $Mg_2(Si,Sn)$ compositions would act as an inhibiting energy contribution to prevent demixing of the material. While this hypothesis needs further confirmation it explains the practical ability to form solid solutions of $Mg_2(Si,Sn)$ at temperatures and compositions within the (incoherent) miscibility gap, resolving a long standing contradiction.

The sample I-600-07 experienced Mg loss, and elemental Si and Sn-rich regions were found after annealing. When Mg loss exceeds the homogeneity range of the $Mg_2(Si,Sn)$ structure with respect to the Mg:*X* ratio, the material starts to decompose, precipitating elemental Si and, in a

second step, also Sn-rich Sn-Mg melt [36, 38]. From Figure 2, under Mg deficiency, three phases, Si-rich Mg_2X (D), Sn-rich Mg_2X (L) and Si (B) are observed. This is in accordance with the ternary phase diagram that these three phases are in equilibrium.

In the sample II-600-05 which was annealed together with Mg flakes, no elemental Si and Sn were observed. The Mg loss is widely suppressed by the extra vapor pressure provided by the Mg flakes so that Mg depletion does not exceed the homogeneity range of Mg_2X. We suppose that in this case, the phase separation will not be assisted by the accumulation of vacancies along the grain boundaries as a consequence of the Mg loss which could break the coherency of the homogenized matrix and release the strain energy. Therefore, the homogenized matrix remains mainly in the coherent state but, in contradiction to the (non-coherent) equilibrium phase diagram, does not decompose by spinodal decomposition. However, this is potentially in contradiction to the result of Yi et al. who found the maximum temperature of the coherent spinodal line above 600 °C [18]. We think that a small uncertainty in the calculation of Yi et al. might explain why a composition of $Mg_2Si_{0.5}Sn_{0.5}$ is not in the spinodal region at 600 °C but it is in the nucleation and growth (binodal) region. Anyway, the observed microstructure could be affected by greatly retarded kinetics. Thus, we interpret the compositions sampled by XRD/EDAX for this sample not as a final state but rather as a snapshot of ongoing evolution. The compositions read from XRD and EDAX are thus not relevant for determining the incoherent equilibrium miscibility gap. Rather, they represent an intermediate situation between the coherent and incoherent gaps. This is well illustrated by the XRD plot of sample II-600-05 (Fig. 1) where most of the material stayed in the coherent matrix forming the main XRD peak (corresponding to $x = 0.51$) whereas small fractions have been demixed forming a small Sn-rich peak (corresponding to $x = 0.12$) and a small Si-rich shoulder of the main peak (corresponding to $x = 0.69$). The main peak's position has shifted, compared to the starting composition, towards the Si-rich side which gives evidence of significant diffusion in the matrix. Preferentially, Sn-rich $Mg_2(Si,Sn)$ precipitates locally where coherency was lost, linked

to counterdiffusion of Sn out of and Si into the matrix. Hence we understand the coexistence of three different $Mg_2(Si,Sn)$ compositions in a sample as caused by a transient process in the material where Sn can easily move along Mg-depleted grain boundaries as it forms a liquid when enriched. Thus, it can easily precipitate in Sn-rich phase domains leaving behind Si-enriched margins neighboring to the grain boundaries which can only slowly balance their concentration gradient to the surrounding matrix by solid state bulk diffusion. Also, Sizov et al. [35] obtained different locally varying Si-rich and Sn-rich compositions, probably affected by different progress levels of Sn diffusion from the grains which can vary locally [35]. We think that Mg loss accelerates the demixing. Usually, diffusion along grain boundaries is stronger than bulk diffusion. Assuming this also for Mg in Mg_2X would result in an ongoing depletion in Mg at the grain boundaries, progressing from outside to inside the sample. It would lead to accumulation of vacancies along the grain boundaries which can act as seeds for relaxation of the coherence strain. Formation of elemental Si precipitates as observed in this work (I-600-07) and as reported by Sizov et al. [35] is another consequence of Mg loss; however we do not interpret Si precipitates as seeds that break coherence. Rather they form when coherence has already been lost. Comparing sample I-600-07, the results in [35] and II-600-05, we conclude that the phase separation can be considerably inhibited by suppressing Mg loss, e.g. by having $Mg_2(Si,Sn)$ samples in an environment with suitable Mg vapor pressure or by using suitable coatings or sealing which block Mg loss from the material. Suppressing Mg loss from $Mg_2(Si,Sn)$ and other Mg containing materials such as Mg_3Sb_2 by suitable coating and/or external Mg vapor pressure during annealing was also previously reported [55-57].

According to calculations of Yi et al. [18], the top of the coherent miscibility gap (elastochemical spinodal line) is located at about 700 °C. Also, according to [18], the composition of $Mg_2Si_{0.5}Sn_{0.5}$ is inside the spinodal lines and not between the spinodal and binodal curves. At 600 °C, the composition of $Mg_2Si_{0.5}Sn_{0.5}$ is thus supposed to be within the

coherent spinodal decomposition region of the Mg_2Si-Mg_2Sn pseudobinary phase diagram [18]. However, we did not observe any coherent spinodal decomposition in our annealing experiments at 600 °C neither in the case where Mg loss occurred (I-600-07) nor under Mg vapor pressure (II-600-05) where the Mg loss was suppressed, and the material was preserved from phase separation by the coherency effect. Therefore, we think that the top temperature of the coherent miscibility gap might be lower than 600 °C, in disagreement to the calculations of Yi et al. [18]. The alternative would be that the gap is shifted in concentration so that the composition of $Mg_2Si_{0.5}Sn_{0.5}$ is outside the coherent miscibility gap.

Yi et al. [18] observed experimentally complete mixing and homogenization of high-energy ball-milled Mg_2Sn and Mg_2Si powders at 720 °C by spark plasma (i.e. current-assisted pressured) sintering (SPS) to form $Mg_2Si_{0.7}Sn_{0.3}$. Also, in our previous work [29], we observed solid solution formation in $Mg_2Si_xSn_{1-x}$ for $x < 0.6$ at 700 °C carrying out high energy ball-milling and homogenization experiments by direct current sintering under pressure. We think that homogenous $Mg_2Si_{0.7}Sn_{0.3}$ in [18] and $Mg_2Si_xSn_{1-x}$ solid solutions with $x < 0.6$ obtained by us [29] through pressure-induced homogenization at 700 °C and above, were formed due to the external strain energy contribution in the pressing process. It is plausible that, due to the grained morphology, the local stress amplitude during the pressing process may even exceed the average external axial pressure. Thus, local stress is clearly reaching magnitudes typical at coherent interfaces even for considerable lattice mismatch. We suppose that this supports the formation of coherent (locked) interfaces in energetically favorable configurations. Also, it is reported that thin liquid films which are formed at the grain boundaries of a material while sintering, can possibly form a diffusion zone between grain boundaries that can lead to formation of coherent adjacent interfaces [51-54]. Therefore, we believe that under the pressured sintering conditions at 700 °C, coherent interfaces will likewise form between the grains of $Mg_2(Si,Sn)$ with equal concentrations as in our experiment, but may even allow for homogenization during sinter pressing from different Mg_2X compositions as reported by Yi et

al. [18]. As a consequence, coherency strain would act as an inhibiting agent to prevent demixing of the material.

Homogenous solid solutions are kept homogeneous also at temperatures much lower than 600 °C due to coherency strain related to the considerable lattice misfit between the Si-rich and Sn-rich Mg_2X but also due to low diffusion constant at lower temperature. Thus, the experimental (coherent) miscibility gap which is relevant for spinodal decomposition from a homogeneous matrix is suppressed down to far below 700 °C. The conclusion that the miscibility gap is suppressed due to coherency strain is in qualitative agreement with the finding of Yi et al. [18] who reported a considerable difference between the coherent (elastochemical) spinodal and incoherent (chemical) miscibility gaps.

Furthermore, in a previous work [29], we found two miscibility gaps at 700 °C and 600 °C carrying out homogenization and diffusion couple experiments, respectively. We think that the results obtained through our diffusion couple experiments conducted at 450–600 °C, and those by Vives et al. [25] correspond to the incoherent equilibrium miscibility gap where the influence of strain can be neglected.

According to Table 3, it is obvious that unlike the samples I-600-07 and II-600-05 which have undergone phase separation, the samples II-525-05 and I-450-30 were stable after annealing and their composition $x = 0.49$ is the same as their nominal composition. Therefore, the results obtained from the sample annealed at 525 °C show that where Mg loss was suppressed, phase separation did not occur. Also, the result obtained in the case of I-450-30 indicates that even if only a proper BN coating is used (without additional Mg vapor pressure), the Mg loss is suppressed at 450 °C, and phase separation could be inhibited. Also, lower diffusion constants at lower temperature could contribute to a slow change of phase constitution here. From the phase diagram reported by Yi et al. [18], it is expected that the main phase separation mechanism at these temperatures should be coherent spinodal decomposition; however we

could not find any experimental evidence from our own experiments or from literature. The observation of homogenous single phase Mg_2X compositions at these temperatures supports the understanding that demixing processes which are expected due to the miscibility gap are inhibited by the coherence strain and the kinetics of the phase separation is substantially retarded. The finding that there is no obvious phase separation at 525 °C and 450 °C is in contradiction to the upper limit of the coherent miscibility gap (720 °C) reported in [18]. We think that either the reported upper limit of the coherent miscibility gap in [18] is overestimated due to e.g. not considering the dependence of elastic moduli of $Mg_2Si_xSn_{1-x}$ on x and on temperature [58] in the calculations of the strain effect, or the phase separation mechanism due to the miscibility gap is very slow at these temperatures. Further analysis and independent calculations on the strain effect are required to find out the reason for this disagreement.

One of our main findings is that avoiding Mg loss by providing Mg vapor pressure around the samples can suppress the phase separation by spinodal decomposition due to the miscibility gap as it, as we assume, will preserve the coherency condition at the grain boundaries. Preventing Mg loss leads to a high chemical stability of $Mg_2Si_{0.5}Sn_{0.5}$ which is close to the $Mg_2(Si,Sn)$ compositions with best thermoelectric performance ($Mg_2Si_{0.3}Sn_{0.7}$ – $Mg_2Si_{0.4}Sn_{0.6}$) [4, 6]. Also, from the thermoelectric application point of view, we believe that adjusting the Mg vapor pressure can even be an adequate tool to adjust the decomposition state of the material and thus affect its microstructure. Consequently, this might be an effective handle to optimize the lattice thermal conductivity [59-61].

Knowing about the combined decomposition and demixing mechanism may help to engineer the microstructure of the material. On an application-relevant time scale, the extent of the Mg loss affects the rate of coherency strain relaxation in the material and thus the rate of the miscibility gap induced phase separation.

5- Conclusions

We find that the phase separation mechanism in $Mg_2(Si,Sn)$ depends sensitively on the Mg concentration, which varies locally in samples due to Mg loss. Suppression of the Mg loss by coating or increased Mg vapor pressure (due to external sources/additional Mg) leads to slowing down or preventing the miscibility gap induced phase separation between 450 °C and 600 °C which is far below the calculated upper limit of the coherent miscibility gap (720 °C) reported by Yi et al. We think that either the actual top of the coherent miscibility gap is far below the calculated value by Yi et al. or the decomposition kinetics is so slow that the phase separation due to the miscibility gap could not be observed below 525 °C within a few days. Providing Mg protecting atmosphere to $Mg_2Si_{0.5}Sn_{0.5}$ can therefore inhibit the Mg loss and the phase separation by spinodal decomposition which could occur due to the relaxation of the coherency strains by accumulation of vacancies along the grain boundaries. This is of high importance for long-term applications since $Mg_2Si_{0.5}Sn_{0.5}$ (being close to the best $Mg_2(Si,Sn)$ compositions) can remain highly stable at elevated temperatures when Mg loss is suppressed. By tuning the Mg vapor pressure around the samples one might be able to engineer the rate of decomposition, and therefore, the amount of the phases precipitated due to a miscibility gap induced phase separation, which can be beneficial for optimizing the thermoelectric properties in $Mg_2(Si,Sn)$ compounds.

Acknowledgments

The authors would like to gratefully acknowledge the endorsement from the DLR Executive Board Member for Space Research and Technology and the financial support from the Young Research Group Leader Program. The authors would also like to thank Silvana Tumminello, Nader Farahi, Dao Y. Nhi Truong (all DLR) and Saneyuki Ohno (JLU Gießen) for their valuable scientific discussions. M. Y. would like to thank for financial support provided by the DFG via the RTG (Research Training Group) 2204 "Substitute Materials for Sustainable

Energy Technologies“ at JLU Gießen. Financial support to K. M. and A. S. is provided by the DAAD. J. de Boor also acknowledges support by the Deutsche Forschungsgemeinschaft (DFG, German Research Foundation) - project number 396709363.

References

[1] S. Gorsse, S. Vivès, P. Bellanger, D. Riou, L. Laversenne, S. Miraglia, D.R.J.M.L. Clarke, Multi-scale architectured thermoelectric materials in the Mg_2(Si, Sn) system, 166 (2016) 140-144.
[2] G.J. Snyder, E.S. Toberer, Complex thermoelectric materials, Nature materials 7(2) (2008) 105-14.
[3] W. Liu, X. Tan, K. Yin, H. Liu, X. Tang, J. Shi, Q. Zhang, C. Uher, Convergence of conduction bands as a means of enhancing thermoelectric performance of n-type $Mg_2Si_{(1-x)}Sn_{(x)}$ solid solutions, Phys Rev Lett 108(16) (2012) 166601.
[4] A. Sankhla, A. Patil, H. Kamila, M. Yasseri, N. Farahi, E. Mueller, J. de Boor, Mechanical Alloying of Optimized Mg_2(Si,Sn) Solid Solutions: Understanding Phase Evolution and Tuning Synthesis Parameters for Thermoelectric Applications, ACS Appl Energ Mat 1(2) (2018) 531-542.
[5] N. Farahi, S. Prabhudev, G.A. Botton, J.R. Salvador, H. Kleinke, Nano- and Microstructure Engineering: An Effective Method for Creating High Efficiency Magnesium Silicide Based Thermoelectrics, ACS Appl Mater Interfaces 8(50) (2016) 34431-34437.
[6] V.K. Zaitsev, M.I. Fedorov, E.A. Gurieva, I.S. Eremin, P.P. Konstantinov, A.Y. Samunin, M.V. Vedernikov, Highly effective$Mg_2Si_{1-x}Sn_x$ thermoelectrics, Physical Review B 74(4) (2006).
[7] T. Dasgupta, C. Stiewe, J. de Boor, E. Müller, Influence of power factor enhancement on the thermoelectric figure of merit in Mg2Si0.4Sn0.6 based materials, physica status solidi (a) 211(6) (2014) 1250-1254.
[8] A. Sankhla, H. Kamila, K. Kelm, E. Mueller, J. de Boor, Analyzing thermoelectric transport in n-type $Mg_2Si_{0.4}Sn_{0.6}$ and correlation with microstructural effects: An insight on the role of Mg, Acta Materialia (2020).
[9] J. de Boor, T. Dasgupta, U. Saparamadu, E. Müller, Z.F. Ren, Recent progress in p-type thermoelectric magnesium silicide based solid solutions, Materials Today Energy 4 (2017) 105-121.
[10] A. Kozlov, J. Gröbner, R. Schmid-Fetzer, Phase formation in Mg–Sn–Si and Mg–Sn–Si–Ca alloys, Journal of Alloys and Compounds 509(7) (2011) 3326-3337.
[11] R. Viennois, C. Colinet, P. Jund, J.-C. Tédenac, Phase stability of ternary antifluorite type compounds in the quasi-binary systems Mg_2X–Mg_2Y (X, Y = Si, Ge, Sn) via ab-initio calculations, Intermetallics 31 (2012) 145-151.
[12] I.-H. Jung, D.-H. Kang, W.-J. Park, N.J. Kim, S. Ahn, Thermodynamic modeling of the Mg–Si–Sn system, Calphad 31(2) (2007) 192-200.
[13] M.G. Kanatzidis, Nanostructured Thermoelectrics: The New Paradigm?†, Chemistry of Materials 22(3) (2010) 648-659.
[14] B.A. Cook, M.J. Kramer, J.L. Harringa, M.-K. Han, D.-Y. Chung, M.G. Kanatzidis, Analysis of Nanostructuring in High Figure-of-Merit $Ag_{1-x}Pb_mSbTe_{2+m}$Thermoelectric Materials, Advanced Functional Materials 19(8) (2009) 1254-1259.
[15] K.F. Hsu, S. Loo, F. Guo, W. Chen, J.S. Dyck, C. Uher, T. Hogan, E.K. Polychroniadis, M.G. Kanatzidis, Cubic $AgPb_{(m)}SbTe_{(2+m)}$: bulk thermoelectric materials with high figure of merit, Science 303(5659) (2004) 818-21.
[16] D. Bilc, S.D. Mahanti, E. Quarez, K.F. Hsu, R. Pcionek, M.G. Kanatzidis, Resonant states in the electronic structure of the high performance thermoelectrics $AgPb_mSbTe_{2+m}$: the role of Ag-Sb microstructures, Phys Rev Lett 93(14) (2004) 146403.
[17] J. Androulakis, C.-H. Lin, H.-J. Kong, C. Uher, C.-I. Wu, T. Hogan, B.A. Cook, T. Caillat, K.M. Paraskevopoulos, M.G. Kanatzidis, Spinodal Decomposition and Nucleation and Growth as a Means to Bulk Nanostructured Thermoelectrics: Enhanced Performance in $Pb_{1-x}Sn_xTe$−PbS, Journal of the American Chemical Society 129(31) (2007) 9780-9788.

[18] S.-i. Yi, V. Attari, M. Jeong, J. Jian, S. Xue, H. Wang, R. Arroyave, C. Yu, Strain-induced suppression of the miscibility gap in nanostructured Mg_2Si–Mg_2Sn solid solutions, Journal of Materials Chemistry A 6(36) (2018) 17559-17570.
[19] D.A. Porter, K.E. Easterling, Phase transformations in metals and alloys (revised reprint), CRC press 2009.
[20] J.W. Doak, C. Wolverton, Coherent and incoherent phase stabilities of thermoelectric rocksalt IV-VI semiconductor alloys, Physical Review B 86(14) (2012).
[21] A.T. Phan, A.E. Gheribi, P. Chartrand, Coherent phase equilibria of systems with large lattice mismatch, Phys Chem Chem Phys 21(20) (2019) 10808-10822.
[22] J.W. Doak, C. Wolverton, V. Ozoliņš, Vibrational contributions to the phase stability of PbS-PbTe alloys, Physical Review B 92(17) (2015).
[23] R. Dalven, Electronic Structure of PbS, PbSe, and PbTe, 28 (1974) 179-224.
[24] M.L. Cohen, J.R. Chelikowsky, Electronic structure and optical properties of semiconductors, Springer Science & Business Media2012.
[25] S. Vivès, P. Bellanger, S. Gorsse, C. Wei, Q. Zhang, J.-C. Zhao, Combinatorial Approach Based on Interdiffusion Experiments for the Design of Thermoelectrics: Application to the Mg_2(Si,Sn) Alloys, Chemistry of Materials 26(15) (2014) 4334-4337.
[26] J.-W. Liu, M. Song, M. Takeguchi, N. Tsujii, Y. Isoda, Transmission Electron Microscopy Study of $Mg_2Si_{0.5}Sn_{0.5}$ Solid Solution for High-Performance Thermoelectrics, Journal of Electronic Materials 44(1) (2015) 407-413.
[27] H. Gao, T. Zhu, X. Liu, L. Chen, X. Zhao, Flux synthesis and thermoelectric properties of eco-friendly Sb doped $Mg_2Si_{0.5}Sn_{0.5}$ solid solutions for energy harvesting, Journal of Materials Chemistry 21(16) (2011) 5933-5937.
[28] Y. Isoda, T. Nagai, H. Fujiu, Y. Imai, Y. Shinohara, Thermoelectric Properties of Sb-doped $Mg_2Si_{0.5}Sn_{0.5}$, 2006 25th International Conference on Thermoelectrics, 2006, pp. 406-410.
[29] M. Yasseri, A. Sankhla, H. Kamila, R. Orenstein, D.Y.N. Truong, N. Farahi, J. de Boor, E. Mueller, Solid solution formation in Mg_2(Si,Sn) and shape of the miscibility gap, Acta Materialia 185 (2020) 80-88.
[30] H. Kamila, P. Sahu, A. Sankhla, M. Yasseri, H.-N. Pham, T. Dasgupta, E. Mueller, J. de Boor, Analyzing transport properties of p-type Mg_2Si–Mg_2Sn solid solutions: optimization of thermoelectric performance and insight into the electronic band structure, Journal of Materials Chemistry A 7(3) (2019) 1045-1054.
[31] J. Bourgeois, J. Tobola, B. Wiendlocha, L. Chaput, P. Zwolenski, D. Berthebaud, F. Gascoin, Q. Recour, H. Scherrer, STUDY OF ELECTRON, PHONON AND CRYSTAL STABILITY VERSUS THERMOELECTRIC PROPERTIES IN Mg_2X(X = Si, Sn) COMPOUNDS AND THEIR ALLOYS, Functional Materials Letters 06(05) (2013).
[32] G.K. Goyal, T. Dasgupta, Effect of Magnesium Content and Processing Conditions on Phase Formation and Stability in $Mg_{2+\delta}Si_{0.3}Sn_{0.7}$, Journal of Electronic Materials 47(3) (2018) 2066-2072.
[33] L. Zhang, X. Chen, Y. Tang, L. Shi, G.J. Snyder, J.B. Goodenough, J. Zhou, Thermal stability of $Mg_2Si_{0.4}Sn_{0.6}$ in inert gases and atomic-layer-deposited Al_2O_3 thin film as a protective coating, Journal of Materials Chemistry A 4(45) (2016) 17726-17731.
[34] G. Skomedal, N.R. Kristiansen, M. Engvoll, H. Middleton, Methods for enhancing the thermal durability of high-temperature thermoelectric materials, Journal of Electronic Materials 43(6) (2014) 1946-1951.
[35] A. Sizov, H. Reardon, B.B. Iversen, P. Erhart, A.E. Palmqvist, Influence of Phase Separation and Spinodal Decomposition on Microstructure of $Mg_2Si_{1-x}Sn_x$ Alloys, Crystal Growth & Design 19(9) (2019) 4927-4933.
[36] I.H. Jung, Applications of thermodynamic calculations to Mg alloy design: Mg-Sn based alloy development, ASM Alloy Phase Diagrams Center 2007.
[37] K. Yin, Q. Zhang, Y. Zheng, X. Su, X. Tang, C. Uher, Thermal stability of $Mg_2Si_{0.3}Sn_{0.7}$ under different heat treatment conditions, Journal of Materials Chemistry C 3(40) (2015) 10381-10387.
[38] M. Yasseri, N. Farahi, K. Kelm, E. Mueller, J. de Boor, Rapid determination of local composition in quasi-binary, inhomogeneous material systems from backscattered electron image contrast, Materialia 2 (2018) 98-103.

[39] H. Kamila, A. Sankhla, M. Yasseri, N.P. Hoang, N. Farahi, E. Mueller, J. de Boor, Synthesis of p-type $Mg_2Si_{1-x}Sn_x$ with x = 0-1 and optimization of the synthesis parameters, Materials Today: Proceedings 8 (2019) 546-555.
[40] J.-i. Tani, H. Kido, First-principles and experimental studies of impurity doping into Mg_2Si, Intermetallics 16(3) (2008) 418-423.
[41] Y.C. Chen, J. Xu, X.H. Fan, X.F. Zhang, L. Han, D.Y. Lin, Q.H. Li, C. Uher, The mechanism of periodic layer formation during solid-state reaction between Mg and SiO_2, Intermetallics 17(11) (2009) 920-926.
[42] J.J. Friel, X-ray and Image Analysis in Electron Microscopy Princeton Gamma-Tech, Princeton, USA, 2003.
[43] R. Saravanan, M.C. Robert, Local structure of the thermoelectric material Mg_2Si using XRD, Journal of Alloys and Compounds 479(1) (2009) 26-31.
[44] V. Glazov, N. Glagoleva, Change in the nature of the chemical bond in compounds of magnesium with Si, Ge, Sn, and Pb upon melting, Inorganic Materials 1 (1965) 989.
[45] D. Kato, K. Iwasaki, Mg-pressure-controlled annealing for tuning Mg content and thermoelectric properties of $Mg_{2-\delta}(Si_{0.5}Sn_{0.5})_{1-x}Sb_x$, Journal of Alloys and Compounds (2020) 157351.
[46] T. Sakamoto, A. Famengo, S. Barison, S. Battiston, S. Boldrini, A. Ferrario, S. Fiameni, T. Iida, Y. Takanashi, M. Fabrizio, Structural, compositional and functional properties of Sb-doped Mg_2Si synthesized in Al_2O_3-crucibles, RSC advances 6(84) (2016) 81037-81045.
[47] G.S. Nolas, D. Wang, M. Beekman, Transport properties of polycrystalline $Mg_2Si_{1-y}Sb_y$ ($0 \le y < 0.4$), Physical Review B 76(23) (2007) 235204.
[48] M. Yasseri, D. Schüpfer, L. Chen, H. Kamila, E. Mueller, J. de Boor, P.J. Klar, Raman spectroscopic study of the optical phonons of $Mg_2Si_{1-x}Sn_x$ solid solutions, physica status solidi (RRL) - Rapid Research Letters (2019).
[49] N. Farahi, C. Stiewe, D.Y.N. Truong, J. de Boor, E. Müller, High efficiency $Mg_2(Si,Sn)$-based thermoelectric materials: scale-up synthesis, functional homogeneity, and thermal stability, RSC Advances 9(40) (2019) 23021-23028.
[50] C. Suryanarayana, Mechanical alloying and milling, Progress in Materials Science 46(1) (2001) 1-184.
[51] Y.-J. Baik, D.N. Yoon, The effect of curvature on the grain boundary migration induced by diffusional coherency strain in mo-ni alloy, Acta Metallurgica 35(9) (1987) 2265-2271.
[52] M. Kuo, R.A. Fournelle, Diffusion induced grain boundary migration (DIGM) and liquid film migration (LFM) in an Al-2.07 wt% Cu alloy, Acta Metallurgica et Materialia 39(11) (1991) 2835-2845.
[53] W.-H. Rhee, D.N. Yoon, The grain boundary migration induced by diffusional coherency strain in Mo□Ni alloy, Acta Metallurgica 37(1) (1989) 221-228.
[54] M. Hillert, On the driving force for diffusion induced grain boundary migration, Scripta metallurgica 17(2) (1983) 237-240.
[55] M. Wood, J.J. Kuo, K. Imasato, G.J. Snyder, Improvement of Low-Temperature zT in a Mg_3Sb_2 - Mg_3Bi_2 Solid Solution via Mg-Vapor Annealing, Adv. Mater. 31(35) (2019) e1902337.
[56] P. Nieroda, K. Mars, J. Nieroda, J. Leszczyński, M. Król, E. Drożdż, P. Jeleń, M. Sitarz, A. Koleżyński, New high temperature amorphous protective coatings for Mg_2Si thermoelectric material, Ceramics International 45(8) (2019) 10230-10235.
[57] D. Kato, K. Iwasaki, M. Yoshino, T. Yamada, T. Nagasaki, Control of Mg content and carrier concentration via post annealing under different Mg partial pressures for Sb-doped Mg_2Si thermoelectric material, Journal of Solid State Chemistry 258 (2018) 93-98.
[58] G. Castillo-Hernandez, M. Yasseri, B. Klobes, S. Ayachi, E. Müller, J. de Boor, Room and high temperature mechanical properties of Mg_2Si, Mg_2Sn and their solid solutions, Journal of Alloys and Compounds (2020) 156205.
[59] P. Bellanger, S. Gorsse, G. Bernard-Granger, C. Navone, A. Redjaimia, S. Vives, Effect of microstructure on the thermal conductivity of nanostructured $Mg_{-2}(Si,Sn)$ thermoelectric alloys: An experimental and modeling approach, Acta Materialia 95 (2015) 102-110.
[60] N. Farahi, S. Prabhudev, G.A. Botton, J.R. Salvador, H. Kleinke, Nano- and Microstructure Engineering: An Effective Method for Creating High Efficiency Magnesium Silicide Based Thermoelectrics, ACS Applied Materials & Interfaces 8(50) (2016) 34431-34437.

[61] W. Liu, X. Tang, H. Li, K. Yin, J. Sharp, X. Zhou, C. Uher, Enhanced thermoelectric properties of n-type $Mg_{2.16}(Si_{0.4}Sn_{0.6})_{1-y}Sb_y$ due to nano-sized Sn-rich precipitates and an optimized electron concentration, Journal of Materials Chemistry 22(27) (2012).